16th World Conference on Earthquake Engineering, 16WCEE 2017

Santiago Chile, January 9th to 13th 2017

Paper N° 2672

Registration Code: S-V1464648321

SOURCES OF LATERAL INSTABILITY AND DEFORMATION LIMITS OF BOUNDARY ELEMENTS OF SPECIAL STRUCTURAL WALLS

C.A. Arteta[1], J.P. Moehle[2]

[(1)] *Assistant Professor, Dept. of Civil and Environmental Engineering, Universidad del Norte, Barranquilla, Colombia, carteta@uninorte.edu.co*

[(2)] *Professor, Dept. of Civil and Environmental Engineering, University of California, Berkeley, moehle@berkeley.edu.*

Abstract

In certain common cases, boundaries at the critical section of multistory reinforced concrete shear wall buildings are expected to undergo large compressive strains that can cause flexural-compression failure. This is especially true for cross-section geometries of L-, C- and T-shaped walls, which, under certain loading conditions, trigger a large tensile force on the flexural-tension side where longitudinal reinforcement is concentrated. This large tensile force, along with the vertical loading, has to be equilibrated by a compression force that can only develop on a narrow stem by further increasing the neutral axis depth. These actions could result in large compressive strains and require a stable plastic response of the narrow stem to be developed. To test the compressive strain limits of code-compliant wall boundaries, a set of 6 full-scale prismatic reinforced concrete rectangular prisms, representative of boundary elements of structural walls with special detailing (per ACI-318), were tested in the laboratory under monotonic incremental axial load until failure. A constraint imposed to the longitudinal and transverse reinforcement layout is that the tested special boundary elements had to be constructible in practice, with no special considerations. This limited the minimum spacing between adjacent layers of transverse reinforcement to 4 in. [100 mm], resulting in tie-spacing-to-longitudinal-bar-diameter ratio (s/d_b) between 3.2 and 4.5. In some specimens, all internal bars were restrained by ties with 135-degree seismic hooks, while in other cases, approximately half the bars were not tied and only restrained by the long leg of the perimeter hoop. Instrumentation was setup to measure axial strains in the cover and core concrete, axial strains along the length of tied and non-tied bars, as well as transverse strain in ties. The out-of-plane displacement and average shortening of the specimens was also recorded. Analysis of the experimental results includes the evaluation of the impact of asymmetric concrete cover spalling and longitudinal bar buckling in the out-of-plane stability of the specimens. Comparison of localized strains measurements with average shortening of the specimens are studied to specify practical deformation limits over various gage lengths along the specimen height. Results suggest that a practical limit in the longitudinal and transverse reinforcement layouts that can be provided might have been reached. The tested specimens showed limited average compressive strain ductility, because after the onset of concrete cover crushing, out-of-plane bending action and bar buckling are triggered. Plastic deformation concentrates over short lengths of approximately two to three wall thicknesses.

Keywords: flexural-compression failure; thin shear walls; compressive strain limit; special boundary element; compression test.

1. Introduction

In certain common cases, boundaries at the critical section of multistory reinforced concrete shear wall buildings are expected to undergo large compressive strains that can cause flexural-compression failure. This is especially true for cross-section geometries of L-, C- and T-shaped walls, which, under certain loading conditions, trigger a large tensile force on the flexural-tension side where longitudinal reinforcement is concentrated. This large tensile force, along with the vertical loading, has to be equilibrated by a compression force that can only develop on a narrow stem, on the flexural-compression side, by further increasing the neutral axis depth. These actions could result in large compressive strains and require a stable plastic response of the narrow stem to be developed. To test the compressive strain limits of code-compliant wall boundaries, a set of 6 full-scale prismatic reinforced concrete rectangular prisms, representative of boundary elements of structural walls with special detailing (per ACI-318 [1]), were tested in the laboratory under monotonic incremental axial load until failure.

The need for special boundary element (SBE) detailing at the edges of structural walls is evaluated according to ACI 318 using either a stress-based or a displacement based approach. By the stress-based approach, SBE detailing is required at wall edges if the extreme fiber compressive stress demand, due to axial load and moment, exceeds 20% of the nominal compressive strength of the concrete (i.e., $\sigma_u \geq 0.2f'_c$). The compressive stress demand is estimated by means of a linear elastic model, using load combinations that include earthquake effects and using gross cross section properties. Alternatively, the displacement-based approach can be applied to walls continuous from the base of the structure to the top of the building, designed to have single critical section for flexure and axial load (Figure 1).

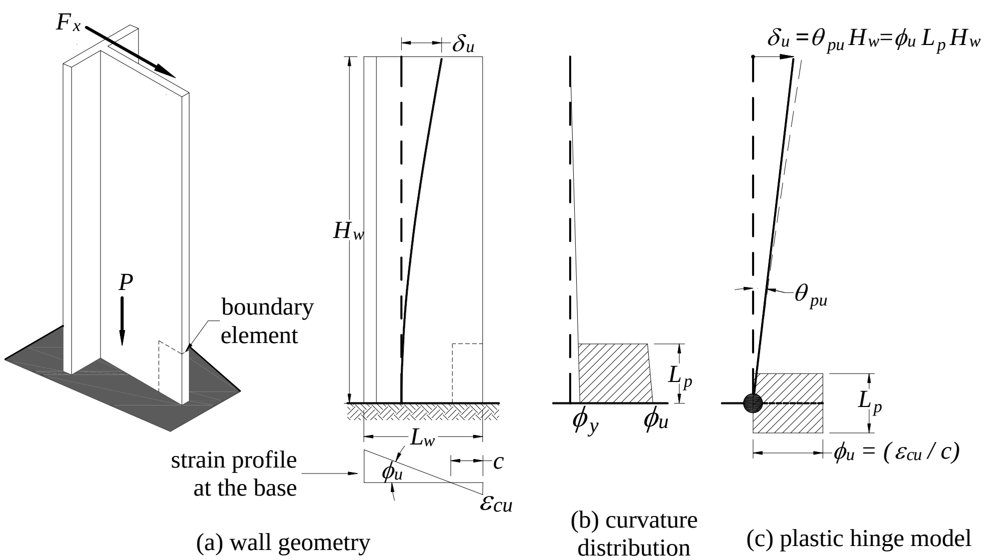

Figure 1 – Relationship between roof displacement and curvature at the critical section of a cantilever wall.

Considering the mechanics of the cantilever wall in Figure 1b, force F_x at the roof displaces the wall δ_u which pushes the critical cross section at the base into its inelastic range. Ignoring shear distortion contributions, and bar slip at the interface of the wall and the base, the roof displacement can be expressed in terms of the flexural deformation distribution along the height of the wall. This model decomposes the curvature distribution into a linear elastic part up to the yield curvature ϕ_y, and a plastic part with constant curvature over plastic length L_p, with maximum inelastic curvature ϕ_u. According to this model, with the Principle of Virtual Work, the roof displacement is estimated as:

$$\delta_u = \frac{\phi_y H_w^2}{3} + (\phi_u - \phi_y) L_p (H_w - \frac{L_p}{2}) \quad (1)$$

where H_w is the height of the wall. The first term in Equation1 is the elastic contribution to the displacement, while the second term is the plastic contribution which occurs as a rigid body motion pivoting at midspan of length L_p. Alternatively, a simplified phenomenological approach directly relates de displacement at the roof with the curvature demands at the critical section level (Figure 1c). This model has been used extensively in the literature [3,4,5] and it is the basis for the development of equation 18.10.6.2 in ACI-318-14 (Equation 4, below) which prescribes requirements of reinforcement detailing at the edge of special structural walls. This simplified model assumes that the plastic hinge is centered at the base of the wall, and that the roof displacement is entirely due to plastic rotation θ_{pu}. Further assuming that curvature ϕ_u at the critical section is uniform along the plastic hinge length, the global roof displacement demand can be expressed in terms of the capacity at the section level as:

$$\delta_u = \theta_{pu} H_w = (\phi_u L_p) H_w \tag{2}$$

It is of interest to relate directly a global demand parameter such as roof drift ratio δ_u/H_w, with a material capacity parameter such as the allowable strain in the maximum fiber in compression ε_{cu}. For this, curvature ϕ_u can be written in terms of uniaxial strain at the critical section, for example $\phi_u = \varepsilon_{cu}/c$, where c is the depth of the neutral axis measured from the extreme fiber in compression. Consequently, Equation 2 can be rearranged as:

$$\frac{\delta_u}{H_w} = \left(\frac{\varepsilon_{cu}}{c}\right) L_p \tag{3}$$

SBE detailing is required at wall edges by the displacement-based approach if:

$$c \geq \frac{L_w}{600\left[\gamma\left(\delta_u / H_w\right)\right]} \tag{4}$$

where c corresponds to the largest neutral axis depth calculated for the factored axial force and nominal moment strength in the direction of the design displacement δ_u; and coefficient γ is 1.0 in ACI-318-11 and 1.5 in ACI-318-14 [2]. Equation 4 stems from Equation 3, by making $L_p = L_w/2$ and $\varepsilon_{cu} = 1/300 \approx 0.0033$. Where SBEs are required, the quantity of transverse reinforcement provided must comply with Equation 6 per ACI-318-11, and Equations 5 and 6 per ACI-318-14:

$$\frac{A_{sh}}{sb_c} \geq 0.3\frac{f'_c}{f_{yt}}\left(\frac{A_g}{A_{ch}} - 1\right) \tag{5}$$

$$\frac{A_{sh}}{sb_c} \geq 0.09\frac{f'_c}{f_{yt}} \tag{6}$$

where s is the center-to-center spacing of transverse reinforcement; b_c is the cross-sectional dimension of the core measured to the outside edges of the transverse reinforcement; A_{sh} is the total quantity of transverse reinforcement provided within spacing s and perpendicular to dimension b_c; A_g is the gross area of the concrete section; A_{ch} is the cross-sectional area of the core measured to the outside edge of the perimeter hoop; f'_c is the specified unconfined concrete compressive strength; and f_{yt} is the specified yield strength of the transverse reinforcement.

2. Specimen geometry, reinforcement, test setup and procedure

Full-scale reinforced concrete prismatic specimens were designed and constructed in accordance with ACI 318-11 provisions for SBEs (i.e. satisfy Equation 6). Specimens BE5 and BE6 also satisfy the more stringent provisions of ACI 318-14 (i.e. also comply with Equation 5). The specimens are representative of the boundary element at the edge of the critical section of a multi-story shear wall. The height, width and thickness of the specimens are: 72 in. [1829 mm], 36 in. [912 mm] and 12 in. [914 mm], respectively. This volume is bounded by two loading reinforced concrete heads constructed monolithically with dimensions 24 x 48 x 20 in. [610 x

1219 x 508 mm] to guarantee a uniform distribution of stresses within the region of interest (Figure 2a). Cover thickness to the outer edge of the perimeter hoop was set to 1.5 in. [38 mm]. Design nominal concrete strength was f'_c = 4.0 ksi [28 MPa] at 28 days and reinforcing steel yield strength was f_y = 60.0 ksi [414 MPa]. All reinforcing steel was compliant with standard ASTM-A706/A706M-9b [6]. A constraint imposed to the longitudinal and transverse reinforcement layout of all specimens is that the tested special boundary elements had to be constructible in practice, with no special considerations. This limited the minimum spacing between adjacent layers of transverse reinforcement to 4 in. [100 mm], resulting in tie-spacing-to-longitudinal-bar-diameter ratio (s/d_b) between 3.2 and 4.5. In some specimens, all internal bars were restrained by ties with 135-degree seismic hooks, while in other cases, approximately half the bars were not tied and only restrained by the long leg of the perimeter hoop.

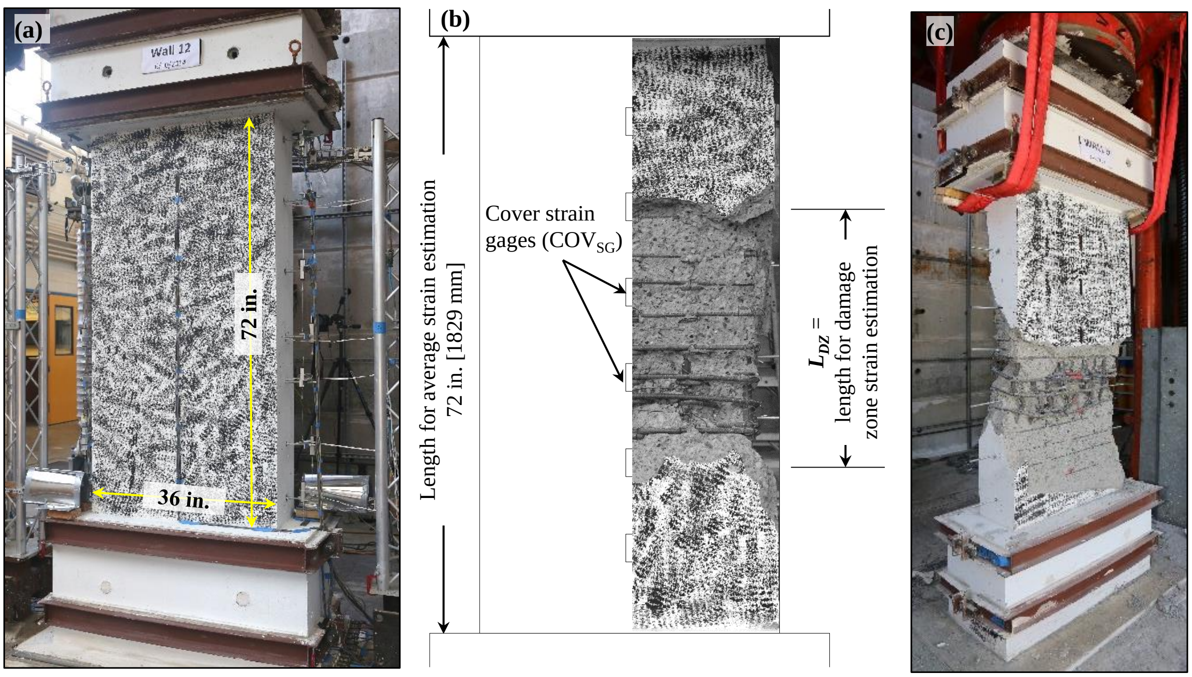

Figure 2 – Test setup and results details: (a) global specimen dimensions and test setup; (b) gage lengths (GL) used for average strain estimations; (c) aspect of specimen BE5 after test conclusion and cleaning up.

Figure 3 shows the general cross section details, and Table 1 contains the geometry, and reinforcement details of the specimens as tested. Instrumentation was setup to measure axial strains in the cover, with concrete strain gages, and axial strains along the length of tied and non-tied bars, with postyield steel strain gages. The out-of-plane displacement of the walls were measured with string potentiometers (‘wirepots’) which monitored several locations along the specimen height. Average shortening of the specimens was also recorded by means of potentiometric displacement transducers. Average strains in the damage zone (L_{DZ}), that is, the length over which spalling and plastic deformation occurred, were also estimated (Figure 2b). The specimens were tested under monotonic uniform compressive loading until failure in the 4-million-pound (17,800 kN) universal testing machine at the *nees@berkeley* laboratory.

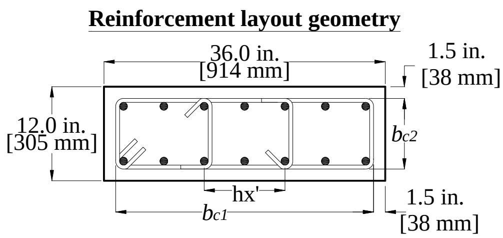

Figure 3 – Cross section geometry and reinforcement layout details.

Table 1 – As tested material properties and reinforcement detailing.

ID	Cross section	f'_c ksi (MPa)	f_y ksi (MPa)	f_{yt} ksi (MPa)	d_b in. (mm)	ρ_l %	s in. (mm)	s / d_b	h'_x in. (mm)	d_{bt} in. (mm)	ρ_{tx} %	ρ_{ty} %	$\rho_{t,ACI1}$ %	$\rho_{t,ACI2}$ %
BE1	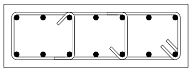	3.8 (26)	68.8 (474)	72.2 (498)	1 (25)	2.6	4.0 (102)	4.0	10.3 (262)	1/2 (13)	1.10	0.60	0.71	0.47
BE2	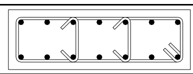	4.0 (28)	69.6 (480)	65.0 (448)	1 (25)	2.6	4.0 (102)	4.0	10.3 (262)	1/2 (13)	1.10	0.60	0.85	0.56
BE3	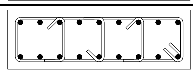	4.2 (29)	67.9 (468)	65.0 (448)	7/8 (22)	2.5	4.0 (102)	4.6	7.7 (196)	1/2 (13)	1.10	0.75	0.89	0.58
BE4	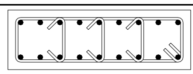	4.4 (30)	67.9 (468)	65.0 (448)	7/8 (22)	2.5	4.0 (102)	4.6	7.7 (196)	1/2 (13)	1.10	0.75	0.91	0.60
BE5	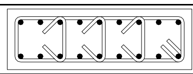	4.6 (32)	76.4 (527)	70.3 (485)	7/8 (22)	2.5	4.0 (102)	4.6	7.7 (196)	5/8 (16)	1.70	**1.16**	**0.90**	0.59
BE6	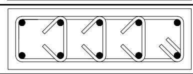	4.4 (30)	77.6 (535)	70.3 (485)	1 1/4 (32)	2.9	4.0 (102)	3.2	7.7 (196)	5/8 (16)	1.70	**1.16**	**0.85**	0.56

f_{yt}: transverse steel yield strength; d_b: longitudinal bar diameter; ρ_l: longitudinal steel ratio (area of longitudinal steel divided by gross cross-sectional area); s: transverse reinforcement spacing; A_{shx}: total cross-sectional area of transverse reinforcement within spacing s, in the long direction of the section; A_{shy}: total cross-sectional area of transverse reinforcement within spacing s, in the short direction of the section; b_{c1}: dimension of the long direction of the section core; b_{c2}: dimension of the short direction of the section core. $\rho_{tx} = A_{shx}/(b_{c2} \cdot s)$ and $\rho_{ty} = A_{shy}/(b_{c1} \cdot s)$ are the provided transverse reinforcement ratios in the two principal directions of the cross section; $\rho_{t,ACI1} = 0.3 f'_c / f_{yt} (A_g / A_{ch} - 1)$ and $\rho_{t,ACI2} = 0.09 f'_c / f_{yt}$ are estimated using "as tested" materials properties.

3. Test results

Figure 2b and 2c depict the typical appearance of the specimens after the test ended. The damage zone (DZ) of the specimens is defined as the length over which cover spalling was measured. The extend of the DZ is presented in Figure 4 as the average spalled-off length of the two larger planes of the prisms. The length of DZ in specimens BE1 to BE6 ranged between 1.8 and $3.1t_w$, with average of $2.5t_w$, where t_w is the thickness of the specimen (i.e. 12 in. [305 mm]). It is worth mentioning that the DZ for specimens BE1 to BE5 comprises a shorter, more damaged length, where bar buckling and loss of concrete core occurred. This length was measured to be in the order of 4 hoop spacing ($1.3t_w$), approximately. Bar buckling was not prevented in these specimens mainly because the flexural stiffness of the long leg of the perimeter hoops was not large enough as to properly restrain the non-tied bars. Bar buckling was only inhibited for specimen BE6, which resulted in a more stable post peak response.

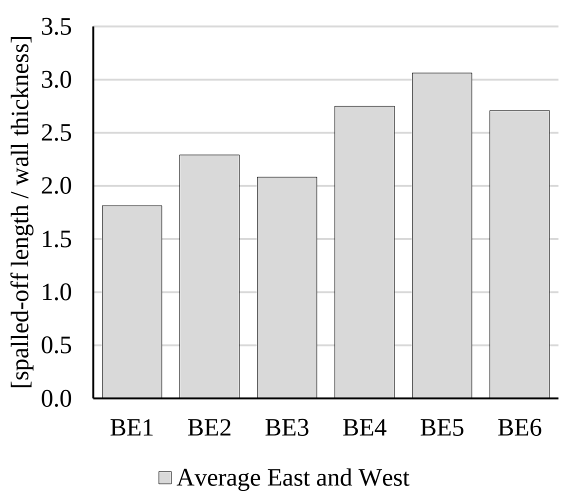

Figure 4 – Average extend of damage in the damage zone.

The force versus average strain relationship of the experiments is shown in Figure 5. The average strain is estimated using the shortening measured between the loading heads, using a gage length (GL) of 72 in. [1829mm]. Additionally, the average strains in the DZ are also presented. The force-shortening relationship of the DZ was recovered using a hybrid model which assumes that the specimens behave as a system of two springs in series. One spring represents the DZ, while the other represents the undamaged zone where no cover spalling was observed. The length of the DZ is consistent with the spalled-off length presented in Figure 4. It is further assumed that the UDZ spring unloads with the initial elastic stiffness after the maximum load is attained, concentrating the plastic strains in the DZ. The softening behavior of the post peak response is apparent and illustrates the dependence of the plastic strain capacity on the gage length over which they are measured. This is explained because the strain distribution along the member height is not uniform due to damage localization [7]. The global response of the specimens B1 to B5 is characterized by a rapid loss of load carrying capacity after the peak load was attained. This maximum load was limited by the onset of concrete cover spalling, after which the specimens were not able to recover the strength. This is explained in part because of the section area reduction due the loss of cover, but also because effective concrete confinement was not achievable due to early bar buckling. Specimen BE6 shows the most stable post peak response because bar buckling was completely inhibited. This specimen failed due to global out-of-plane lateral instability at an average global axial strain of approximately 2.0%.

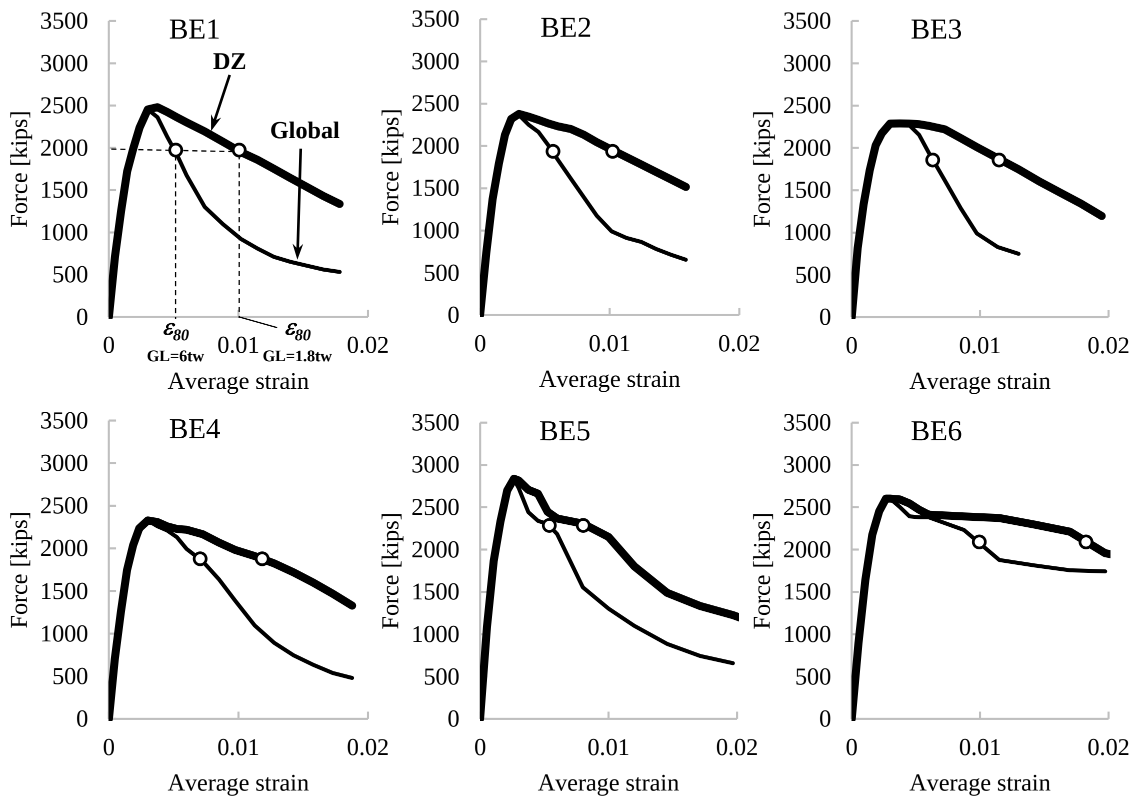

Figure 5 – Force versus deformation response at the global and at the damaged-zone level.

3.1. Out-of-plane action

Out of plane displacement profiles, normalized by the thickness of the wall are presented in Figure 6b for the three instances of the response highlighted in Figure 6a: (i) at maximum load, (ii) at 90 percent of maximum load after the peak load is attained and (iii) at 80 percent of maximum load after the peak load is attained. Out-of-plane instability is triggered by the asymmetric nature of concrete cover spalling, in which one face of the specimen crushes instants before the opposite side. This behavior promotes an overturning moment generated by the eccentricity of the applied axial load and the migrated centroid of the cross-section. An empirical axial force

– moment interaction diagram for the test evolution of specimen BE5 is constructed and compared with the theoretical PM failure surfaces in Figure 6c. The PM interaction surfaces are constructed assuming actual material properties at the moment of the test for two cases of cross section geometry: the outer orbit assumes the full cross section is available to sustain flexural compression demands and the inner one assumes half of the concrete cover has spalled off. The moment in the empirical PM curve is approximated as the applied axial load times the out-of-plane displacement at the critical section. It is observed that the maximum axial load is attained with relatively small lateral displacement. After the onset of concrete cover spalling, the overturning moment grows rapidly and the empirical PM curve transitions from the outer orbit to the inner one, before a pronounced drop in axial load carrying capacity occurs.

3.2. Onset of bar buckling

Instrumentation of the longitudinal bars allowed monitoring strains at discrete locations along their height. Strain gages in tied and nontied bars were glued in the point of the bar cross section farthest away from the cover (i.e., adjacent to the concrete core). Figure 7 shows the evolution of the axial load (left axis) and longitudinal strains of a nontied bar (right axis) versus the normalized average shortening of specimen BE5. Rebar compressive strains shown are from three adjacent strain gages located within the buckling length of a nontied bar. The onset of bar buckling is defined as the instant at which either of the external strain gages within the buckling length starts unloading. Strain gage (sgBar5) starts unloading at around 1% of longitudinal average strain in the bar. This instant also coincides with an abrupt change in the slope of the middle strain gage (sgBar6), which is located around midspan of the buckling length, hence recording compressive strains at a faster rate. The top strain gage unloads at larger strains because its location does not exactly coincide with the extreme of the buckling length, but instead is located closer to midspan. On the force versus average strain curve, it is observed that after the onset of bar buckling there is a sudden drop of 10% in axial force carrying capacity.

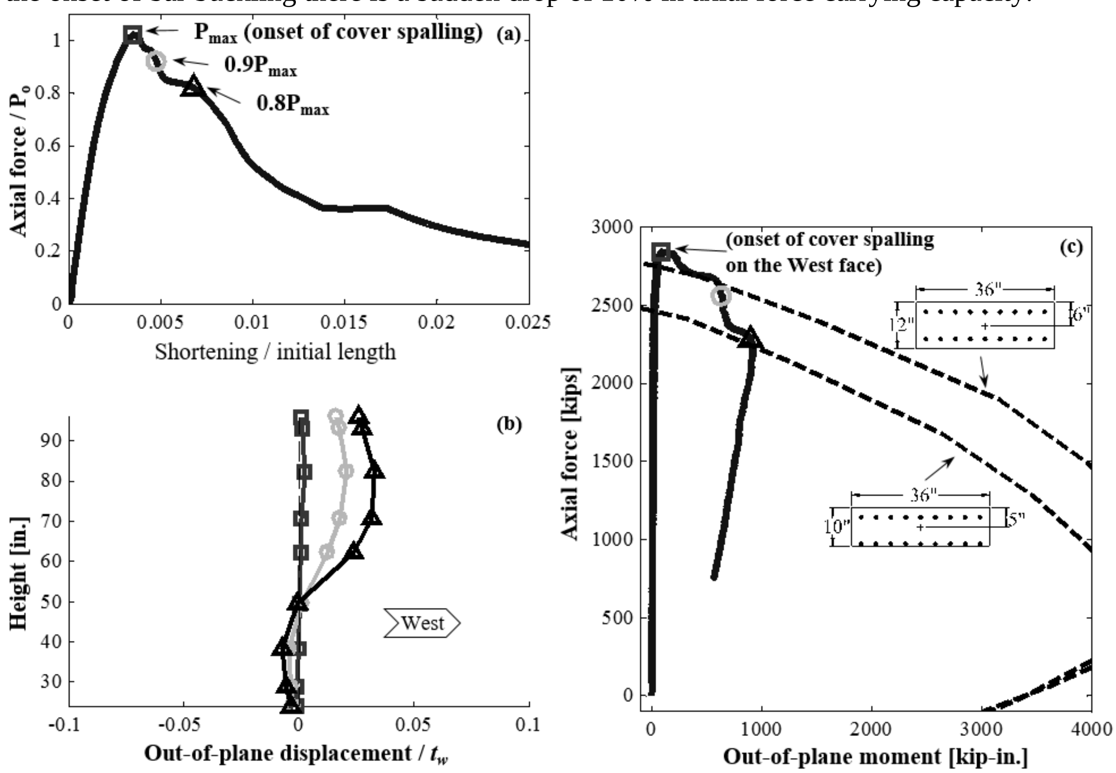

Figure 6 – Specimen BE5 test evolution: (a) force-average strain relation; (b) normalized out-of-plane displacement profile; (c) axial force – moment interaction during the test evolution of specimen BE5 [1 kips= 4.45 kN; 1kip-in.= 0.11 kN-m; 1in. = 25.4 mm).

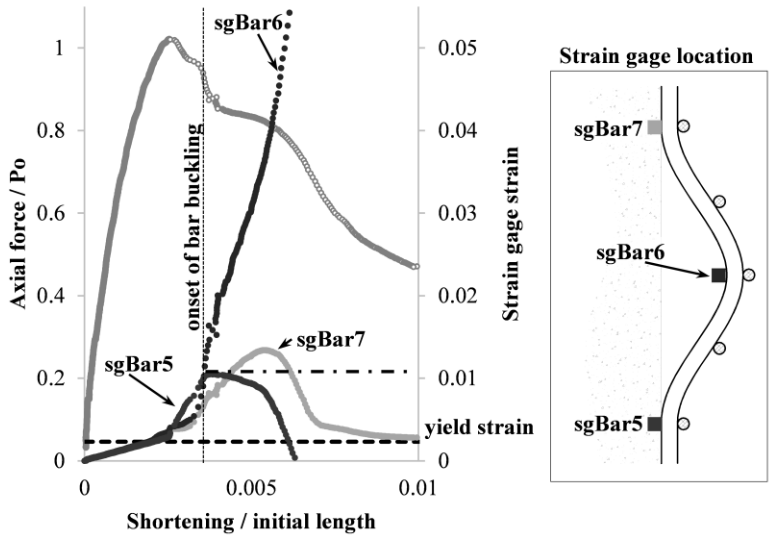

Figure 7 – Strains along the buckling length of a nontied bar.

3.3. Usable strain limit

To further study the post peak response of the specimens, the strain capacity at the 80% strength level (ε_{80}) is analyzed (see markers in Figure 5). This is the strain associated to a 20% drop in load carrying capacity after the peak load is attained. Strength losses beyond the aforementioned limit are not considered in favor of conservatism. Figure 8 depicts the ε_{80} values of each specimen paired with the corresponding gage length over which they were measured. A linear transition is assumed between the strains measured within the two different gage lengths. Assuming an average GL of 2.5t_w for the DZ, the ε_{80} strain capacity of the specimens is bounded between 1.0% and 1.8%. For the larger GL of 6t_w, these values are smaller and bounded between 0.5% and 1.0%. An apparent improved behavior with respect to specimens BE1 and BE2 (which had the lowest transverse reinforcement ratio in the through-the-thickness direction of the specimens) is observed for specimen BE6 for which bar buckling was completely inhibited. This is explained because all longitudinal bars within its cross-section were restrained with a stiff seismic tie (i.e.d_{bt} = 5/8 in. [15.9 mm]), and because the larger longitudinal bar diameter used resulted in a ratio s/d_b equal to 3.1.

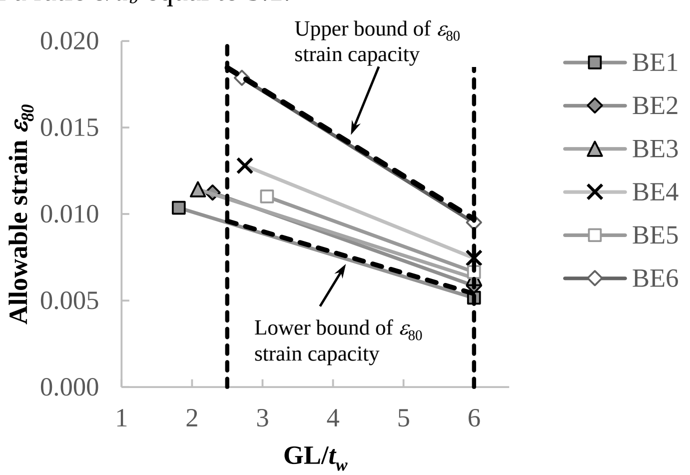

Figure 8 – Usable strain limits for two gage lengths.

4. Implications of the results

Where flexural compression yielding is expected, the strain limits presented above are useful for estimating usable curvature values of multistory shear walls with comparable boundary elements at the extreme of their critical section. The proposed lower and upper limits (ε_{max}) in Figure 7 can be parametrized in terms of GL/t_w as:

$$\varepsilon_{\max} = b - m\left(GL/t_w \right) \tag{7}$$

where b and m are respectively, 0.013 and 0.0012 for the lower bound, and 0.025 and 0.0025, for the upper bound (valid in the range $2.5 \le GL/t_w \le 6$). To contextualize the implications of the proposed strain limits in terms of a gage length, the relationship between global deformation capacity (e.g. roof drift) and demand at the section level (e.g. compressive strain in the extreme fiber in compression) presented in Equation 3, can be rewritten in terms of the allowable strain demand of Equations 7 as:

$$\frac{\delta_u}{H_w} = \left(\frac{\varepsilon_{\max}}{c}\right) L_p = \left(\frac{b - m\left(GL/t_w \right)}{c}\right) L_p \tag{8}$$

Because of the softening nature of the response in compression, it is necessary to guarantee objectivity in the response. That is, the gage length associated to the strain capacity proposed must be close to the region extent over which plastic deformation occurs in the wall. This ensures consistency between the local (i.e. at the section level) and global deformations (i.e. roof displacement), and can be approximated by making the plastic hinge length equal to the gage length as $L_p = t_w(GL/t_w)$, resulting in:

$$\frac{\delta_u}{H_w} = \left(\frac{\varepsilon_{\max}}{c}\right) L_p = \left(\frac{b - m\left(GL/t_w \right)}{c}\right) \left(GL/t_w \right) t_w \tag{8}$$

Figure 9 compares the response of a hypothetical reinforced concrete wall of total height H_w, with boundary elements at the critical section having similar reinforcement characteristics and assumed axial deformation capabilities as those in specimens BE1 to BE6. Given a selected plastic hinge length, the y-axis values in Figure 9 are associated to the roof drift ratio capacity. It is observed that although the maximum usable compressive strain, ε_{max}, decreases with increasing gage length (therefore, plastic hinge length, according to the discussion above), the displacement capacity of the wall increases with increasing plastic hinge length up to gage length $5t_w$, approximately, plateauing or falling on a soft decreasing slope up to $L_p = 6t_w$ thereafter.

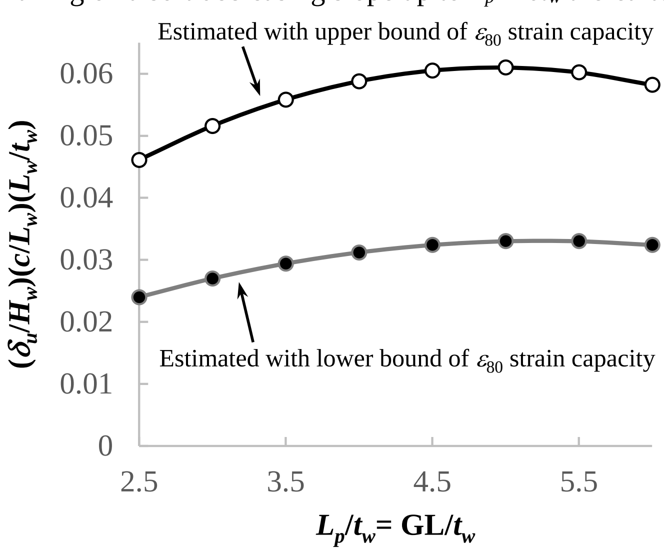

Figure 9 – Drift capacity versus gage length.

The trends shown offer an alternative view of the global-displacement versus local-strain problem that deviates from the traditional thought that plastic displacement capacity should be independent from the plastic hinge length selected. This is so because the plastic hinge length and the compressive strain capacity are coupled, and because of the built-in local-deformation (e.g. curvature) and global-deformation (e.g. roof drift) consistency without the need for material regularization. Specifically, the material model strains, including the post peak softening portion, are measured over a gage length equal to the assumed plastic hinge. Regularly, when dealing with softening response at the section level, engineers select (or are restricted to) certain plastic hinge length and adjust the concrete material post peak softening slope in what is called material regularization. This is done to ensure that displacement capacity is independent from the plastic region extension, which is often constraint to have certain length depending on the modeling scheme [8, 9]. For example, if nonlinear finite-element-type of analysis is used, the mesh needs to be of certain maximum size to ensure the answer converges to a stable solution. For softening behavior, this means that modeled plasticity will be constraint to extend over a small area, therefore, exacerbating the local strain demand for a given global displacement. It is difficult for the material model gage length and the mesh size to agree, requiring adjustments of the material model post peak portion to ensure adequate plastic displacement capacity at the global level. When this is done, the displacements at the roof of a wall in cantilever and the strains at the at the base (critical section) are not consistent and reverse regularization must be performed to estimate the strain demand at the material level.

5. Final comments

Experimental results of six prismatic reinforced concrete elements under pure compression are presented. The specimens are representative of the flexural compression zone of multistory special shear walls, and are compliant with design specifications for special boundary elements per ACI-318-11. Analysis of the experimental results included the evaluation of the impact of asymmetric concrete cover spalling and longitudinal bar buckling in the out-of-plane stability of the specimens. Comparison of localized strains measurements with average shortening of the specimens were studied to specify practical deformation limits over various gage lengths along the specimen height. Results suggest that a practical limit in the longitudinal and transverse reinforcement layouts that can be practically provided might have been reached. The tested specimens showed limited average compressive strain ductility, because after the onset of concrete cover crushing, out-of-plane bending action and bar buckling are triggered. Plastic deformation concentrates over short lengths of approximately two to three times the specimen thickness. Strain capacity at the 80% post peak strength level were bounded between 1.0% and 1.8% for gage length of 2.5-times the specimen thickness. For larger gage lengths (e.g. 6-times the specimen thickness), these values are smaller and bounded between 0.5% and 1.0%. The tests of specimen BE5 provided insight into the instability of thin walls. In summary, the axial load carrying capacity of slender prismatic element can be limited by asymmetric concrete cover spalling due to induced out-of-plane moment. This in turns, instantaneously exacerbates the compressive strain demand on the flexural compression side of the spalled section, triggering buckling of the longitudinal reinforcement and further reducing the axial capacity of the cross section. The results also showed that bars restrained by the flexural stiffness of perimeter hoops develop plastic buckling at longitudinal local bar strains of 1% approximately for a ratio between the hoop spacing and the longitudinal bar diameter, s/d_b, of 4.6. Implementation of a simple plastic hinge model, in which the plastic hinge length and the strain capacity are coupled, showed that longer plastic hinge lengths are associated with larger displacement capacity, albeit the reduction in usable strain capacity.

6. Acknowledgements

Two rebar fabricator supported this research: ERICO (LENTON) and CMC Rebar Fabricators provided part of the reinforcing steel used in the laboratory specimens; their support is acknowledged with gratitude. The research presented here has been supported in part by the National Institute of Standards and Technology through the ATC 94 project and by the National Science Foundation under award number 1208192. Opinions, findings, conclusions and recommendations in this document are those of the author and do not necessarily represent those of the sponsors.

7. Copyrights

8. References

[1] ACI-Committee-318. (2011). Building Code Requirements for Structural Concrete and Commentary (ACI 318-11). Farmington Hills, MI: American Concrete Institute.

[2] ACI-Committee-318. (2014). Building Code Requirements for Structural Concrete and Commentary (ACI 318-14). Farmington Hills, MI: American Concrete Institute.

[3] Moehle, J. P. 1992. Displacement-based design of RC structures subjected to earthquakes. Earthquake spectra. Vol. 8, No. 3, pp. 403-428.

[4] Wallace, J. W. & Orakcal, K. 2002. ACI 318-99 provisions for seismic design of structural walls. ACI Structural Journal, Vol. 99, No. 4, pp. 499-508.

[5] Priestley, M.J.N., Calvi, G.M. y Kowalsky, M.J. 2007. Displacement Based Seismic Design of Structures. IUSS Press. Pavia, 721 pp.

[6] ASTM-A706/A706M-9b. 2009. Standard Specification for Low-Alloy Steel Deformed and Plain Bars for Concrete Reinforcement (pp. 6). West Conshohocken, PA: ASTM International.

[7] Markeset, G., & Hillerborg, A. (1995). Softening of Concrete in Compression - Localization and Size Effects. Cement and Concrete Research, 25(4), 702-708.

[8] Coleman, J., & Spacone, E. (2001). Localization issues in force-based frame elements. Journal of Structural Engineering, 127(11), 1257-1265.

[9] Scott, M. H., & Hamutçuoğlu, O. M. (2008). Numerically consistent regularization of force-based frame elements. International Journal for Numerical Methods in Engineering, 76(10), 1612-1631.